COMMUNICATION

Check for updates

Photoisomerization-controlled wavelength-tunable plasmonic lasers†

Shuang Wen,[ab] Wu Zhou,[ab] Zhiyuan Tian, [iD][b] Yongli Yan [iD] *[a] and Yong Sheng Zhao [iD] *[ab]

We demonstrate photoisomerization-controlled wavelength-tunable plasmonic lasers by integrating spiropyran derivative-doped PMMA films with two-dimensional Ag nanoparticle arrays. The controllable transformation between spiropyran derivatives and its isomers with different refractive indices by photoexcitation allows for a dynamical and continuous change of the refractive index in the host PMMA film, which is able to tune the lattice plasmon resonance, and hence the lasing wavelength. This result opens up a new avenue for engineering wavelength tunable plasmonic lasers toward practical photonic integration.

Plasmonic lasers that can deliver intense coherent light with ultrafast dynamics and ultrasmall mode volumes have attracted extensive attention for their important roles in ultra-compact and fast photonic devices.[1–6] A dynamical and continuous tunability of lasing wavelength would promote the application of plasmonic lasers in high performance wavelength-division multiplexing (WDM) and on-chip spectroscopy.[7–9] Since the output of plasmonic lasers is determined by both the emission of the gain media and resonance of the plasmonic cavity,[10,11] various strategies based on energy-level tailoring of the gain materials[12–17] and rational structure design of the plasmonic cavities[18–21] have been proposed for tunable plasmonic lasers. Nevertheless, most of these approaches hinder the possibility of continuous tuning in a ready-made system. The sensitivity of plasmonic resonance to the refractive index of the dielectric surroundings affords us a convenient alternative to adjust the lasing wavelength through varying the refractive index.[22–24] Integrating plasmonic lattices within microfluidic channels and flowing liquid gain materials with different refractive indices has been proven to be very effective in dynamically

modulating the output wavelength of plasmonic lasers.[25] Unfortunately, the reliance on liquid gain materials results in poor compactness and integrability of the devices, which restricts the practical applications in on-chip integration.

This problem can be circumvented by exploiting solid gain materials with an adjustable refractive index. However, most of the ready-made solid systems suffer from an unchangeable refractive index due to the fixed material composition. Organic photochromic compounds provide an ideal platform to realize *in situ* modulation of the refractive index because the structural rearrangement through unimolecular electrocyclization upon light excitation can create isomers with different refractive indices.[26,27] Such a photoisomerization process is usually reversible and thus allows for an adjustable concentration of the isomers, realizing a dynamical tuning of effective refractive index.[28,29] Therefore, developing a device consisting of a high-gain photochromic compound and plasmonic lattices offers possibilities to realize a controllable modulation of plasmonic lasing.
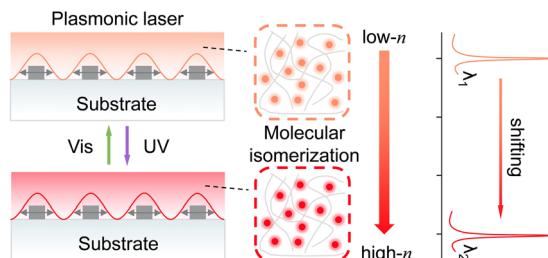
In this work, we demonstrated wavelength-tunable plasmonic lasers based on photoisomerization-activated change of the refractive index in two-dimensional Ag nanoparticle arrays covered by a spiropyran derivative doped PMMA film. The spiropyran derivative is controllably transformed into a merocyanine isomer with different refractive indices under exposure to ultraviolet (UV) light, which enabled precise tuning of the refractive index of the host PMMA film, and therefore a shift of the lattice plasmon resonances in the plasmonic arrays. As a result, dynamically and continuously adjustable plasmonic lasing was realized with the merocyanine isomers offering optical gain and the plasmonic arrays providing optical feedback. Our results enlighten the design of tunable plasmonic lasers based on the external stimuli induced change of material optical properties, and create new opportunities for tiny coherent lasers in integrated photonic circuits.

The design principle for the tunable plasmonic lasers based on a photoisomerization-activated change of refractive index is illustrated in Scheme 1. A photochromic compound-doped polymer film is selected as the gain layer and covered onto a

[a] *Key Laboratory of Photochemistry, Institute of Chemistry, Chinese Academy of Sciences, Beijing 100190, China*

[b] *School of Chemical Sciences, University of Chinese Academy of Sciences, Beijing 101408, China*

† Electronic supplementary information (ESI) available: Experimental details and other characterizations. See DOI: https://doi.org/10.1039/d3cc01505j

Scheme 1 Schematic illustration for wavelength-tunable plasmonic lasers based on photoisomerization-activated change of refractive index.

two-dimensional metal nanoparticle array to construct a plasmonic laser. The metal nanoparticle array consisting of periodically arranged metal nanoparticles on a silica substrate is used to provide optical feedback for laser oscillation. The localized surface plasmons (LSPs) of individual nanoparticles couple strongly with Bragg diffractive modes propagating in the array, creating the surface lattice resonances (SLRs).[30] The SLR modes are highly related to the environmental refractive index due to the Bragg diffractive condition. Therefore, the lasing wavelength determined by SLR modes can be tuned by changing the environmental refractive index. Here, the refractive index of the top doped polymer film can be precisely modulated through controllable transformation of the photochromic compound into its isomer, which has a higher refractive index than its original counterpart. As a result, a continuous wavelength shift of the plasmonic laser can be realized through the photoisomerization process.

Here, poly(methyl methacrylate) (PMMA) was selected as the host polymeric matrix due to its high material compatibility and good optical transparency in the visible (vis) and near-infrared (NIR) spectral ranges.[31] $1',3'$-Dihydro-$1',3',3'$-trimethyl-6-nitro-spiro[$2H$-1-benzopyran-$2,2'$-($2H$)-indole] (BIPS) (Fig. 1a), as a typical photoisomerizable dye, was chosen to incorporate into

Fig. 1 (a) Reversible photoisomerization of BIPS between spiropyran and merocyanine forms. (b) Energy diagram for the concentration-dependent ICT process of BIPS-MC. (c) PL spectra from a 20 wt% BIPS@PMMA film at different UV exposure times. (d) Refractive indices of the BIPS@PMMA film with increasing exposure time to UV light.

the PMMA to simultaneously provide optical gain and adjust the refractive index of the PMMA film.[29,32] The photoisomerization induced change of the refractive index was explored in BIPS-doped PMMA films (BIPS@PMMA) by photoexcitation (Fig. S1, ESI†). Under irradiation with UV light, spiropyran derivative BIPS can transform into merocyanine isomers (BIPS-MC) (Fig. S2, ESI†).[33] The emission of BIPS-MC@PMMA continuously shifts toward longer wavelength with the increase of the doping concentration (Fig. S3, ESI†), showing strong intramolecular charge-transfer (ICT) character and concentration-dependent ICT energy levels (Fig. 1b).[34] As illustrated in Fig. 1c, the PL spectra from a 20 wt% BIPS@PMMA film red-shift as the exposure time to UV light increases, suggesting the piecemeal transformation from BIPS to BIPS-MC isomers. Correspondingly, the absorbance of the identical film is enhanced with increasing UV exposure time (Fig. S4, ESI†), further confirming the occurrence of photoisomerization. As a result, the effective refractive index of the BIPS@PMMA film monotonically rises with a gradual accumulation of BIPS-MC since the BIPS-MC has a higher refractive index than BIPS (Fig. 1d). It is known from Fig. S5 (ESI†) that the formed BIPS-MC amounts and the refractive index change synchronously with the UV exposure time, demonstrating that the change of refractive index arises from the photoisomerization process. In addition, BIPS-MC can transform back to BIPS upon exposure to Vis light and the emission wavelengths of BIPS and BIPS-MC remain almost unchanged after a dozen continuous cycles (Fig. S6, ESI†), indicating the excellent reversibility of the BIPS molecular photoisomerization. The controllable transformation between low-refractive index BIPS and high-refractive-index BIPS-MC provides a potential possibility for dynamically tunable plasmonic lasers.

High quality plasmonic cavities, with the resonance wavelength accurately matching the gain range of BIPS-MC, are indispensable for the realization of plasmonic lasers (Fig. 2a).[35–37] Since the lattice plasmon resonance wavelength depends heavily on lattice geometry (including the morphology and arrangement of individual particles) and environmental refractive index, we used the finite-difference time-domain (FDTD) methods to exactly simulate the lattice plasmon resonance wavelength and therefore give useful guidance to the structural design. The environmental refractive index was set to be 1.51, which is the same as the measured refractive index of the BIPS@PMMA film. It is found that an Ag nanoparticle array, comprising patterned particles with a diameter of 80 nm and height of 50 nm as well as a spacing of 460 nm is the optimal cavity because of its narrow resonance peak at 695 nm shown in the calculated transmission spectra (Fig. 2b, red line), which overlaps well with the PL emission of BIPS-MC. Fig. 2c presents the simulated electric field ($|E|^2$) distribution maps of the array at the resonant condition. An intense nanolocalized field concentrates on the edge of individual nanoparticles, indicating a large local density of optical states that can promote the stimulated emission processes. The standing wave pattern shown in the phase distribution maps (Fig. 2d) is attributed to the Bragg diffraction in the plane of the array, demonstrating
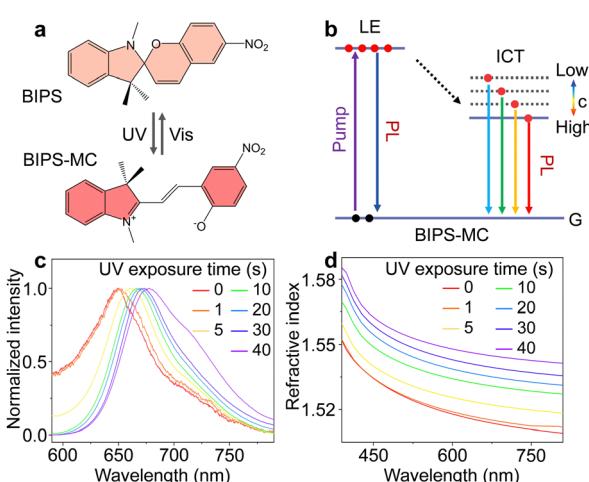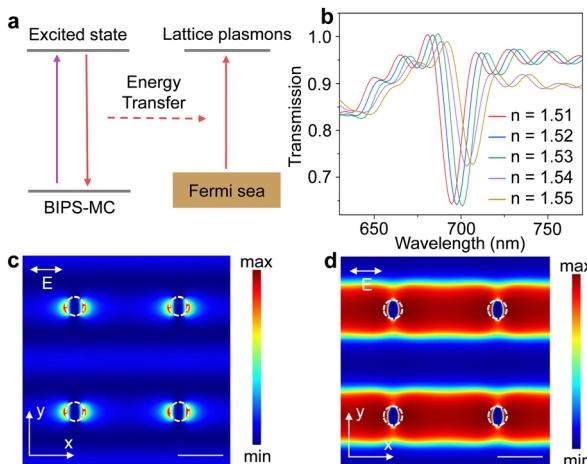
Fig. 2 (a) Energy diagram for the coupling between the BIPS-MC and the lattice plasmons. (b) FDTD-simulated transmission spectra of the Ag nanoparticle array in different dielectric environments ($n = 1.51$–1.55). (c) FDTD-simulated distribution map of electric field intensity ($|E|^2$) of the Ag nanoparticle array at the x–y plane. (d) FDTD-simulated phase distribution map of the Ag nanoparticle array at the x–y plane. Scale bars in (c) and (d): 200 nm.
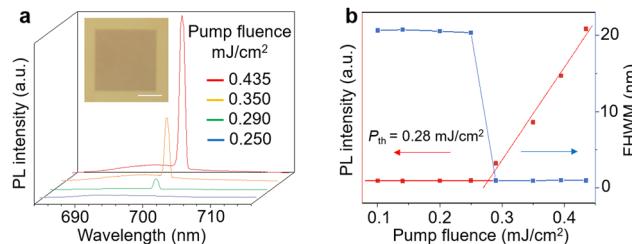

Fig. 3 (a) PL spectra of the BIPS@PMMA film-covered Ag nanoparticle array at different pump fluences. Inset: Bright-field microscopy image of the fabricated device. Scale bar is 50 μm. (b) Emission intensity (red) and FWHM (blue) as a function of pump fluence.

that plasmonic lattices can provide effective optical feedback for lasing. It is worth mentioning that the simulated lattice plasmon resonances red-shift with the increasing environmental refractive index (Fig. 2b), affording us an opportunity to achieve wavelength-tunable plasmonic lasers.

The well-designed Ag nanoparticle arrays were fabricated through a standard electron beam lithography (Fig. S7, ESI†).[19] The scanning electron microscopy (SEM) image (Fig. S8, ESI†) indicates that Ag nanoparticles with a diameter of 80 nm and height of 50 nm were periodically arrayed on the silica surface with a spacing of 460 nm, which is consistent with the predesigned geometric size to ensure high-quality plasmonic modes. Afterwards, a thin SiO_2 layer was evaporated onto the nanoparticle arrays to protect Ag from oxidation. Finally, the nanoparticle arrays were covered by a 20 wt% BIPS@PMMA film with a thickness of 300 nm, which is thin enough to ensure the full photoisomerization of BIPS molecules around Ag nanoparticles (Fig. S9, ESI†).

The fabricated devices were characterized with a home-built far-field micro-photoluminescence system to explore the lasing behaviour (Fig. S10, ESI†). The plasmonic device with a 5 nm-thick SiO_2 layer exhibits excellent laser performances due to a desirable balance between the interactions of Ag nanoparticles and BIPS-MC molecules (Fig. S11, ESI†). Fig. 3a summarizes the PL spectrum of the identical devices as a function of pump fluence under the excitation of a pulsed laser beam (400 nm, 100 fs, 1 kHz) at normal incidence. At relatively low pump fluences (<0.28 mJ cm^{-2}), the PL spectra are dominated by broad spontaneous emissions. With increasing pump fluence, a sharp and intense peak emerges ($\lambda = 695$ nm) close to the position of the lattice plasmon resonance ($\lambda = 697.5$ nm), which manifests lattice plasmon-assisted lasing action. The emission intensity shows a nonlinear increase and the FWHM dramatically decreases down to 0.91 nm at a critical threshold of $P_{th} = 0.28$ mJ cm^{-2} (Fig. 3b).

The clear threshold behaviour further confirms lasing action in the plasmonic lattice.[38]

Based on the discussions in Fig. 1d and 2b, the lasing wavelength of the BIPS@PMMA film-covered Ag nanoparticle array can be further tuned under UV-Vis irradiation because of the photoisomerization-activated change of refractive index. With increasing exposure time to UV light, the lasing wavelength of the BIPS@PMMA film-covered Ag nanoparticle array was continuously tuned from 697.5 nm to 710.5 nm (Fig. 4a). Fig. 4b shows the plot of the lasing wavelength and refractive index of the BIPS@PMMA film *versus* exposure time to UV light. The similar change trend of the lasing wavelength and refractive index with exposure time demonstrates that the tuning of the lasing wavelength arises from the change of refractive index through the photoisomerization process. Here, the photothermal effect of Ag nanoparticles on the refractive index variations and lasing wavelength shift is ruled out due to the non-resonant excitation of the ultrashort pulsed laser.[39] The laser wavelength tuning is fully reversible, namely that the laser wavelength returns to its original position under continuous Vis exposure
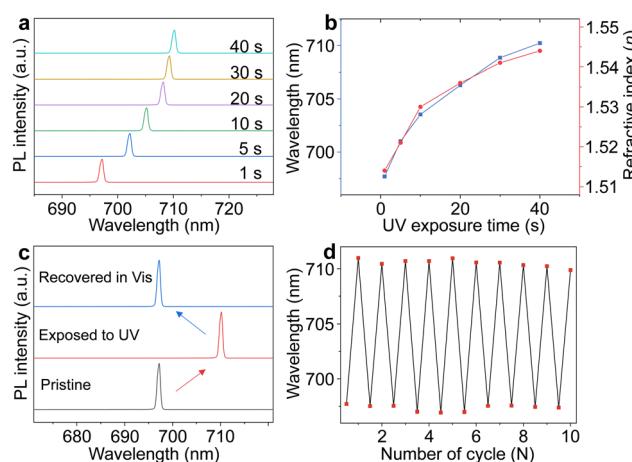

Fig. 4 (a) Time-dependent lasing spectra of the BIPS@PMMA film-covered Ag nanoparticle array on exposure to UV light. (b) Plots of the lasing wavelength and refractive index of the BIPS@PMMA film-covered Ag nanoparticle array *versus* time of exposure to UV light. (c) Lasing spectra of the BIPS@PMMA film-covered Ag nanoparticle array under alternate irradiation with UV and Vis light. (d) Plot of the lasing wavelength *versus* switching cycles.

(Fig. 4c and Fig. S12, ESI†). Furthermore, we examined the repeatability of the optically controlled wavelength tuning of the plasmonic laser by measuring the laser wavelengths and intensities after multiple cycles of alternating UV and Vis irradiation. The laser wavelength and tuning range remain nearly unchanged (Fig. 4d) and the laser intensity maintains 92.7% of its initial value (Fig. S13, ESI†) after a dozen of continuous UV-Vis exposure cycles, fully demonstrating the excellent reversibility and reproducibility of the as-fabricated tunable plasmonic laser. With such excellent performance, the dynamically and continuously tunable plasmonic laser promises to be widely used in the fields of ultrasensitive sensing, on-chip spectroscopy and optical interconnects.[40]

In summary, we demonstrated wavelength-tunable plasmonic lasers in Ag nanoparticle arrays covered by a spiropyran derivative-doped PMMA film. Under UV light exposure, the spiropyran molecules transformed into merocyanine isomers, which could be reversed through Vis light irradiation. Such a photoisomerization process led to a real-time tuning of the refractive index in the PMMA film since the merocyanine derivatives possess a higher refractive index. The change of the refractive index in the PMMA film resulted in a redshift of the lattice plasmon resonance. On this basis, we realized a dynamical and continuous modulation of lasing wavelength with the merocyanine isomers offering optical gain and the Ag nanoparticle arrays providing optical feedback. This result highlights the huge potential of the photochromic molecules in tunable plasmonic lasers for all-optical functional plasmonic devices.

Conflicts of interest

There are no conflicts to declare.

Notes and references

1 M. A. Noginov, G. Zhu, A. M. Belgrave, R. Bakker, V. M. Shalaev, E. E. Narimanov, S. Stout, E. Herz, T. Suteewong and U. Wiesner, *Nature*, 2009, **460**, 1110–1112.
2 R. F. Oulton, V. J. Sorger, T. Zentgraf, R. M. Ma, C. Gladden, L. Dai, G. Bartal and X. Zhang, *Nature*, 2009, **461**, 629–632.
3 R.-M. Ma, R. F. Oulton, V. J. Sorger and X. Zhang, *Laser Photonics Rev.*, 2013, **7**, 1–21.
4 S. I. Azzam, A. V. Kildishev, R. M. Ma, C. Z. Ning, R. Oulton, V. M. Shalaev, M. I. Stockman, J. L. Xu and X. Zhang, *Light: Sci. Appl.*, 2020, **9**, 90.
5 Y. Liang, C. Li, Y. Z. Huang and Q. Zhang, *ACS Nano*, 2020, **14**, 14375–14390.
6 Z. Wu, J. Chen, Y. Mi, X. Sui, S. Zhang, W. Du, R. Wang, J. Shi, X. Wu, X. Qiu, Z. Qin, Q. Zhang and X. Liu, *Adv. Opt. Mater.*, 2018, **6**, 1800674.
7 X. Yang, Z. Shan, Z. Luo, X. Hu, H. Liu, Q. Liu, Y. Zhang, X. Zhang, M. Shoaib, J. Qu, X. Yi, X. Wang, X. Zhu, Y. Liu, L. Liao, X. Wang, S. Chen and A. Pan, *ACS Nano*, 2020, **14**, 3397–3404.
8 S. S. Deka, S. Jiang, S. H. Pan and Y. Fainman, *Nanophotonics*, 2020, **10**, 149–169.
9 D. Wang, M. R. Bourgeois, W.-K. Lee, R. Li, D. Trivedi, M. P. Knudson, W. Wang, G. C. Schatz and T. W. Odom, *Nano Lett.*, 2018, **18**, 4549–4555.
10 B. Wang, P. Yu, W. Wang, X. Zhang, H. C. Kuo, H. Xu and Z. M. Wang, *Adv. Opt. Mater.*, 2021, **9**, 2001520.
11 Y. J. Li, Y. Lv, C. L. Zou, W. Zhang, J. Yao and Y. S. Zhao, *J. Am. Chem. Soc.*, 2016, **138**, 2122–2125.
12 J. M. Taskinen, A. J. Moilanen, H. Rekola, K. Kuntze, A. Priimagi, P. Törmä and T. K. Hakala, *ACS Photonics*, 2020, **7**, 2850–2858.
13 C. Li, Z. Liu, J. Chen, Y. Gao, M. Li and Q. Zhang, *Nanophotonics*, 2019, **8**, 2091–2110.
14 Q. Zhang, Q. Shang, J. Shi, J. Chen, R. Wang, Y. Mi, W. Du, C. Shen, R. Ma, X. Qiu, X. Liu and T. C. Sum, *ACS Photonics*, 2017, **4**, 2789–2796.
15 Y. Lv, Y. J. Li, J. Li, Y. Yan, J. Yao and Y. S. Zhao, *J. Am. Chem. Soc.*, 2017, **139**, 11329–11332.
16 Y. J. Lu, C. Y. Wang, J. Kim, H. Y. Chen, M. Y. Lu, Y. C. Chen, W. H. Chang, L. J. Chen, M. I. Stockman, C. K. Shih and S. Gwo, *Nano Lett.*, 2014, **14**, 4381–4388.
17 X. Liu, Q. Zhang, J. N. Yip, Q. Xiong and T. C. Sum, *Nano Lett.*, 2013, **13**, 5336–5343.
18 S. Pourjamal, T. K. Hakala, M. Necada, F. Freire-Fernandez, M. Kataja, H. Rekola, J. P. Martikainen, P. Törmä and S. van Dijken, *ACS Nano*, 2019, **13**, 5686–5692.
19 D. Wang, W. Wang, M. P. Knudson, G. C. Schatz and T. W. Odom, *Chem. Rev.*, 2018, **118**, 2865–2881.
20 D. Wang, A. Yang, W. Wang, Y. Hua, R. D. Schaller, G. C. Schatz and T. W. Odom, *Nat. Nanotechnol.*, 2017, **12**, 889–894.
21 J. M. Winkler, M. J. Ruckriegel, H. Rojo, R. C. Keitel, E. De Leo, F. T. Rabouw and D. J. Norris, *ACS Nano*, 2020, **14**, 5223–5232.
22 J. E. Park, R. Lopez-Arteaga, A. D. Sample, C. R. Cherqui, I. Spanopoulos, J. Guan, M. G. Kanatzidis, G. C. Schatz, E. A. Weiss and T. W. Odom, *ACS Nano*, 2022, **16**, 3917–3925.
23 H.-S. Chen, J.-Y. Wang, S.-S. Yeh, C.-D. Chen and H.-Y. Lin, *Appl. Phys. Lett.*, 2012, **100**, 011102.
24 S. Zhang, L. Chen, Y. Huang and H. Xu, *Nanoscale*, 2013, **5**, 6985–6991.
25 A. Yang, T. B. Hoang, M. Dridi, C. Deeb, M. H. Mikkelsen, G. C. Schatz and T. W. Odom, *Nat. Commun.*, 2015, **6**, 6939.
26 A. Bianco, S. Perissinotto, M. Garbugli, G. Lanzani and C. Bertarelli, *Laser Photonics Rev.*, 2011, **5**, 711–736.
27 Y. Shi, W. H. Steier, L. Yu, M. Chen and L. R. Dalton, *Appl. Phys. Lett.*, 1991, **58**, 1131–1133.
28 C. Zhang, F. J. Shu, C. L. Zou, H. Dong, J. Yao and Y. S. Zhao, *Adv. Mater.*, 2023, **35**, 2300054.
29 C. Qiao, C. Zhang, Z. Zhou, H. Dong, Y. Du, J. Yao and Y. S. Zhao, *Angew. Chem., Int. Ed.*, 2020, **59**, 15992–15996.
30 T. K. Hakala, H. T. Rekola, A. I. Vakevainen, J. P. Martikainen, M. Necada, A. J. Moilanen and P. Törmä, *Nat. Commun.*, 2017, **8**, 13687.
31 Y. Wang, V. D. Ta, K. S. Leck, B. H. Tan, Z. Wang, T. He, C. D. Ohl, H. V. Demir and H. Sun, *Nano Lett.*, 2017, **17**, 2640–2646.
32 L. Persano, E. Mele, A. Athanassiou, R. Cingolani and D. Pisignano, *Chem. Mater.*, 2006, **18**, 4171–4175.
33 C. Qiao, C. Zhang, Z. Zhou, J. Yao and Y. S. Zhao, *CCS Chem.*, 2022, **4**, 250–258.
34 H. Huang, Z. Yu, D. Zhou, S. Li, L. Fu, Y. Wu, C. Gu, Q. Liao and H. Fu, *ACS Photonics*, 2019, **6**, 3208–3214.
35 A. Fernandez-Bravo, D. Wang, E. S. Barnard, A. Teitelboim, C. Tajon, J. Guan, G. C. Schatz, B. E. Cohen, E. M. Chan, P. J. Schuck and T. W. Odom, *Nat. Mater.*, 2019, **18**, 1172–1176.
36 W. Zhou, M. Dridi, J. Y. Suh, C. H. Kim, D. T. Co, M. R. Wasielewski, G. C. Schatz and T. W. Odom, *Nat. Nanotechnol.*, 2013, **8**, 506–511.
37 H. Wei, X. Yan, Y. Niu, Q. Li, Z. Jia and H. Xu, *Adv. Funct. Mater.*, 2021, **31**, 2100889.
38 F. F. Xu, Y. J. Li, Y. Lv, H. Dong, X. Lin, K. Wang, J. Yao and Y. S. Zhao, *CCS Chem.*, 2020, **2**, 369–375.
39 M. Strasser, K. Setoura, U. Langbein and S. Hashimoto, *J. Phys. Chem. C*, 2014, **118**, 25748–25755.
40 A. Pan, W. Zhou, E. S. P. Leong, R. Liu, A. H. Chin, B. Zou and C. Z. Ning, *Nano Lett.*, 2009, **9**, 784.